# Multichannel interferometry using high-order rotating diffraction gratings

John Howard, George B. Warr, and Peter Dodds
*Plasma Research Laboratory, Research School of Physical Sciences and Engineering, Australian National University, G.P.O. Box 4, Canberra, A.C.T. 2601, Australia*

(Presented on 18 March 1992)

We report the successful construction and operation of a far-infrared (337 $\mu$m) interferometer based on a multiple-order diffraction grating wheel. On reflection from the wheel circumference, the incident laser beam is diffracted into a number ($\sim 12$) of approximately equal intensity high-order beams. Since the Doppler offset of the beams is proportional to the diffraction order, information encoded by the spatially distinct beams is multiplexed in the frequency domain. This allows simultaneous multichannel phase shift information to be obtained using only a single detector.

## I. INTRODUCTION

The phase shift suffered by a probing far-infrared laser beam on passage through a plasma is a measure of the plasma electron density integrated along the line-of-sight.[1] Interferometric measurements of the phase shift for beams at a number of viewing angles and impact parameters allow, in principle, the density profile to be recovered approximately using tomographic techniques.[2] Having in mind application of such techniques to the $H$-1 helical-axis stellarator under construction at the Australian National University (ANU), two new types of multichannel density interferometer based on scanning and multibeam rotating diffraction gratings have been recently proposed.[3–5]

The first type of interferometer makes use of a multisectored blazed disc grating. Upon wheel rotation, the beam incident on the circumferential edge is diffracted sequentially through a range of discrete angles determined by the grating constant of the illuminated sector. Because of this multiplexing in time, many spatial channels can be obtained using a single laser beam and detector. An interferometer based on this principle has been recently successfully installed on the TORTUS tokamak at the University of Sydney.[6] Time resolution for the scanning interferometer is, however, necessarily limited by the maximum attainable wheel speed.

In this article we report the successful construction and operation of a multiorder dual-polarization rotating grating interferometer. The beam incident on the circumference in this case is diffracted simultaneously into a range of orders determined by the grating profile design. The $m$th-order angle of diffraction $\theta_m$ for a plane electromagnetic wave ($\lambda_0=2\pi/k_0$, $\omega_0=ck_0$) incident at angle $\theta_i$ on an infinite plane grating having groove spacing $d=2\pi/K$ is given by

$$k_0 \sin \theta_m = k_0 \sin \theta_i + mK. \tag{1}$$

Upon wheel rotation, and for reflection in the plane of the wheel, the radiation is Doppler shifted in angular frequency by

$$\Omega_m = mKR\omega, \tag{2}$$

where $R$ is the wheel radius and $\omega$ is the wheel angular frequency. If the grating groove profile can be tailored to generate a fan array of $N$ sufficiently closely spaced probe beams $\{\theta_m; m=m_1,m_2,\ldots,m_N\}$, each of the resulting distinct plasma spatial channels will be tagged by $\Omega_m$. This restores the continuous time resolution, for, under conditions specified later, all the probe beams can be mixed in a single detector and the phase information $\phi_m(t)$ carried by the $m$th-order beam retrieved unambiguously.

In Sec. II, we compare measured and computed reflection profiles for a particular groove geometry. This is followed by a description of the Michelson-type interferometer arrangement in Sec. III. Because of its dual polarization capability, the instrument can be used as a polarimeter for the measurement of birefringent and optically active media. In Sec. IV we briefly discuss optical mixing detection and demodulation of the interferogram and report successful imaging measurements of a birefringent quartz target using 12 distinct beams.

## II. REFLECTED BEAM PROFILES

As detailed in Ref. 5 the groove profile for the multiorder grating is constructed of $N$ flat "subfacets," with adjacent subfacets incrementally inclined to reflect specularly into the next highest order. The typical groove profile shape is shown as an inset to Fig. 2. The power distribution among the reflected propagating orders, is estimated by solving the idealized problem of plane wave diffraction from a perfectly conducting plane grating using the mode-matching method of Yasuura.[7,8]

We examine the reflection from a sector having six grooves of width $d=6$ mm cut on the circumference of a test grating wheel of radius 150 mm and thickness 20 mm. The grooves are illuminated by a 10 mW hydrogen cyanide (HCN) laser source ($\lambda_0=337$ $\mu$m) focused onto the wheel at an incidence angle $\theta_i=-45°$. The grooves are designed to diffract the beam into a fan array of beams clustered about the grating normal.

Measured diffracted beam profiles at $z=0.4$ m for the H polarization ($E$ perpendicular to the grooves) are presented in Fig. 1. As noted in Ref. 5, there can be significant ($\sim 50\%$) variation in the distribution of power into the reflected orders depending on the position of the groove surface relative to the incident beam. This may be due to the small size of the illuminated region (spot diameter at

 0034-6748/92/104965-03$02.00  

intensity $1/e \sim 5.2$ mm) compared with the groove width. Near-field effects may also be important since the measurement distance is not significantly greater than the Fresnel length $L_F \sim d^2/\lambda_0 \approx 100$ mm. We examine the consequences of this modulation in Sec. IV. The experimental profiles are the average of six power measurements taken at angles equispaced over the full angle subtended by the 6 mm groove at the wheel center. The profile has been normalized so that the sum of the energies in the measured orders is unity. The sets of vertical bars superimposed on the measured profiles in Fig. 1 show the computed relative power distribution among the diffracted orders for $\theta_i = -45°$. Details of the computation, which take no account of the wheel curvature, are given in Ref. 5. The 12 most intense beams occupy a fan of angle 40° about the grating normal. There is reasonable agreement between the simple plane wave simulations and experiment. The results of more extensive Gaussian beam simulations will be presented elsewhere.

## III. THE INTERFEROMETER

A schematic diagram of the interferometer is shown in Fig. 2. The 45° diagonal polarizer (DP) splits the horizontally polarized incident laser beam into diagonally polarized probe and local oscillator beams. The expanded probe beam is focused by lens L3 ($f=260$ mm) onto the cylindrical diffraction grating. The position and focal length of L3 are chosen to compensate the negative curvature of the grating surface[3] so that the beams diffracted into the discrete orders are approximately collimated and spatially separated. The cylindrical lens (CL) compensates for the asymmetric reflection properties of the grating.

The cylindrical mirror (CM) returns the probe beams along their incident path so that they execute a double pass of the grating. It is calculated that approximately 10% of the power in each of the return beams is diffracted back along the incident beam path and collected by L3. The double pass conveniently recombines the probe beams in a single beam that is easily collected and focused onto the detector. Furthermore, the dual pass of the rotating grating doubles the Doppler shift of the beams. In principle, this increases the information bandwidth available to the discrete carriers to $\pm f_0$ where $f_0 = R\omega/d$ is the frequency of

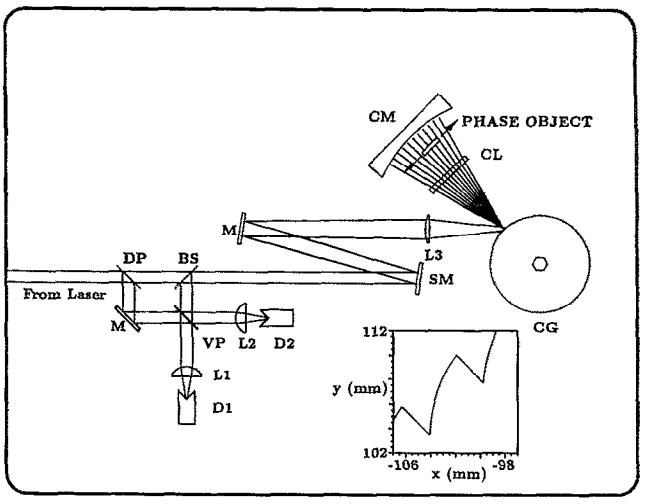


FIG. 2. Schematic scale drawing of the dual polarization, multiorder interferometer. Key: BS—beam splitter, CG—rotating cylindrical diffraction grating, CL—cylindrical lens, CM—cylindrical mirror, D1, D2—Schottky diode detectors, DP—45° polarizer, L1 and L2—$f=10$ cm lenses, L3—$f=26$ cm lens, M—plane mirror, SM—$f=-140$ cm spherical mirror, VP—vertical polarizer. The inset shows the groove shape at the position of beam incidence.

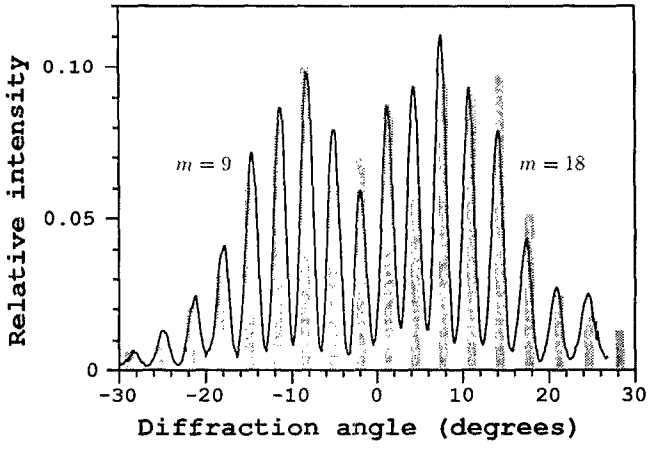


FIG. 1. Measured (solid line) and calculated (shaded) power distribution among the diffracted orders for H polarization illumination of the $d=6$ mm grating surface at $-45°$ angle of incidence.

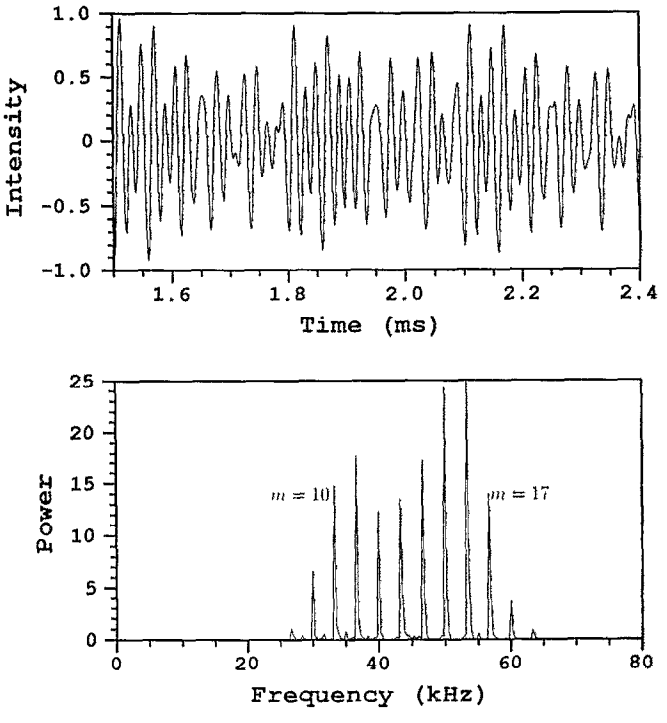


FIG. 3. Part of the interferogram recorded for the horizontally polarized probe beam (detector D2) showing three periods at the groove frequency $f_0$ and (b) the corresponding power spectrum for the complete ~4 ms burst of fringes. The associated diffraction orders are labeled on the figure.

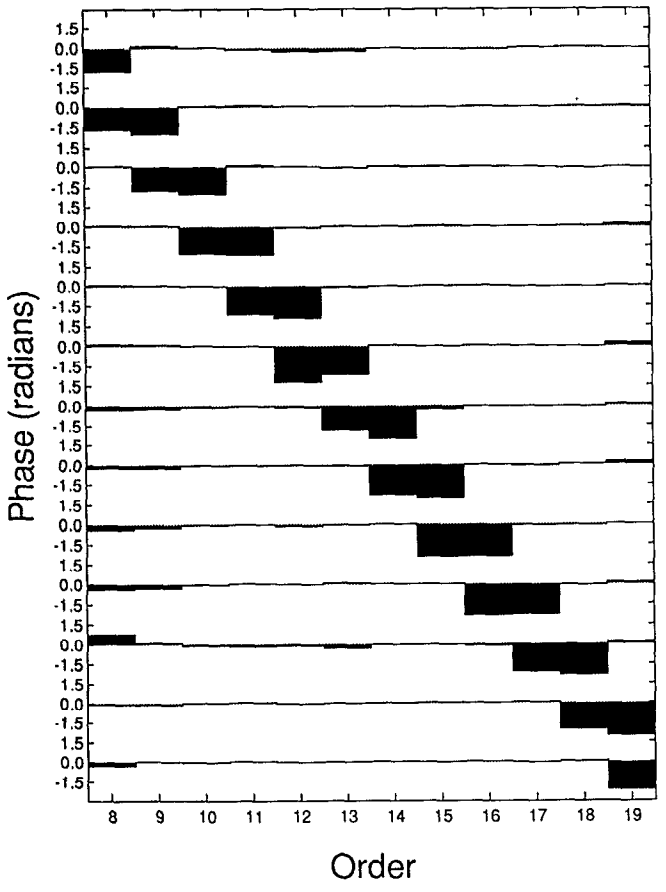


FIG. 4. Multibeam imaging of a 4.5 cm wide birefringent quartz target.

grooves past the incident beam (typically $f_0 \sim 40$ kHz for wheel rotation speeds of 100 Hz).

The total return power is sampled by a beam splitter and directed to the vertical polarizer (VP) where it is resolved into its horizontal and vertical components and combined with the local oscillator beam. Finally, the orthogonal probe and local oscillator beams are caused to interfere using a half-wave plate prior to detection using Schottky corner-cube mixers D1 (for the vertically polarized probe beam) and D2 (for the horizontally polarized beam). The power cross talk between the two probe polarizations is measured to be less than 2%.

## IV. PHASE IMAGING

The interferometer can be used to sense the relative phase shift between the orthogonally polarized probe beams caused by insertion of a birefringent quartz target. Note that this polarimetric phase measurement is insensitive to noise due to vibrations.

Figure 3(a) shows a portion of the fringe burst recorded by detector D2 and Fig. 3(b) its associated power spectrum. The signals are bandpass filtered between 10 and 160 kHz prior to digitization at 200 kHz rate. Since there is no significant power above 100 kHz, aliasing due to undersampling is not a problem. We note the existence of pronounced spectral peaks corresponding to mixing of the diffracted orders $m_1 = 8$ to $m_N = 19$ with the unshifted local oscillator beam. The width of the spectral peaks is determined solely by the $\sim 4$ ms duration of the fringe burst while their separation is found to satisfy Eq. (2) to better than one part in $10^4$. In passing, we note that the alignment of the return optics is optimized by monitoring the real-time power spectrum of the interferogram using a transient power spectrum analyzer.

The observed modulation of the reflected intensity with presentation of the grooves noted in Sec. II, is evident in the power spectrum predominantly as sidebands residing at $\pm f_0$ from the carrier. Because of the double grating pass, this modulation fortunately does not cause interference with adjacent carriers. The sidebands apparent in Fig. 3, though of relatively low power, nevertheless reduce the practically available information bandwidth.

Using the signal from D1 as a frequency reference for that from D2, a digital complex demodulation technique[9] has been used for extraction of the relative phase between the orthogonal probe beams. The rectangular quartz target is 4.5 cm wide and is translated, on a shot-to-shot basis, across the curved surface of the return mirror. The quartz surface is unpolished, resulting in significant insertion loss ($\sim 50\%$ for a double pass) and an attendant degradation of the extracted phase signal to noise. Nevertheless, as seen in Fig. 4, a clear phase image of the moving target can be obtained from the digitized interferograms. Within the $f_0 \sim 1.5$ kHz bandwidth for these experiments, the phase noise increases from about 3° for the strongest channels to $\sim 10°$ for the extreme orders. The use of a higher power source should allow improvements in phase noise by at least an order of magnitude.

## ACKNOWLEDGMENTS

We wish to thank K. Kawahata for his generous assistance in the fabrication of the corner-cube Schottky diode mixers and S. M. Hamberger for provision of the excellent facilities required to carry out this work. This work was in part supported by funding from the Australian Institute of Nuclear Science and Engineering. The Authors also wish to acknowledge financial support received from the Australian Research Council (J.H.) and the Australian Commonwealth Scholarship and Fellowship Plan (G.B.W.).

[1] D. Veron, in *Infrared and Millimeter Waves*, edited by K. J. Button (Academic, New York, 1979), Vol. 2, pp. 69–135.
[2] J. Howard, E. J. Doyle, G. Reibeiz, R. L. Savage, W. A. Peebles, and N. C. Luhmann, Jr., Rev. Sci. Instrum. **59**, 2135 (1988).
[3] J. Howard, Rev. Sci. Instrum. **61**, 1086 (1990).
[4] J. Howard, M. Bowden, A. J. Campbell, G. Cornish, I. S. Falconer, B. W. James, S. M. Hamberger, L. E. Sharp, and G. B. Warr, Conference Proceedings, IAEA Technical Committee Meeting on 2D and 3D Time and Space Resolved Tokamak Diagnostics. Nagoya, Japan, November, 1990.
[5] J. Howard, Appl. Opt. **31**, 1419 (1992).
[6] B. W. James, (private communication).
[7] H. Ikuno and K. Yasuura, IEEE Trans. Antennas Propag. AP **21**, 657 (1973).
[8] T. Matsuda, and Y. Okuno, J. Opt. Soc. Am. A 7, 1693 (1990).
[9] D. W. Choi, E. J. Powers, R. D. Bengston, G. Joyce, D. L. Brower, N. C. Luhmann, Jr., and W. A. Peebles, Rev. Sci. Instrum. **57**, 1989 (1986).